
CAUSAL LIFTING OF NEURAL REPRESENTATIONS: ZERO-SHOT GENERALIZATION FOR CAUSAL INFERENCES

Riccardo Cadei¹, Ilker Demirel^{2,†}, Piersilvio De Bartolomeis^{3,†}, Lukas Lindorfer¹,
Sylvia Cremer¹, Cordelia Schmid⁴, Francesco Locatello¹

¹Institute of Science and Technology Austria (ISTA)

²Massachusetts Institute of Technology (MIT)

³Department of Computer Science, ETH Zurich

⁴INRIA, Ecole Normale Supérieure, CNRS, PSL Research University

[†]*Equal contribution.*

ABSTRACT

In many scientific domains, the cost of data annotation limits the scale and pace of experimentation. Yet, modern machine learning systems offer a promising alternative—provided their predictions yield correct conclusions. We focus on *Prediction-Powered Causal Inferences* (PPCI), i.e., estimating the treatment effect in a target experiment with unlabeled factual outcomes, retrievable zero-shot from a pre-trained model. We first identify the conditional calibration property to guarantee valid PPCI at population level. Then, we introduce “causal lifting”, a new causal lifting constraint transferring validity across experiments, which we propose to enforce in practice in *Deconfounded Empirical Risk Minimization*, our new model-agnostic training objective. We validate our method on synthetic and real-world scientific data, offering solutions to instances not solvable by vanilla Empirical Risk Minimization and invariant training. In particular, we solve zero-shot PPCI on the ISTAnt dataset for the first time, fine-tuning a foundational model on our replica dataset of their ecological experiment with a different recording platform and treatment.

1 Introduction

Artificial Intelligence (AI) systems hold great promise for accelerating scientific discovery by providing flexible models capable of automating complex tasks. We already depend on deep learning predictions across various scientific domains, including biology [Jumper et al., 2021, Tunyasuvunakool et al., 2021], medicine [Elmarakeby et al., 2021, Mullowney et al., 2023], sustainability [Zhong et al., 2020, Rolnick et al., 2022], and social sciences [Jerzak et al., 2022, Daoud et al., 2023]. While these models offer transformative potential for scientific research, their black-box nature poses new challenges, especially when used to analyze new experimental data. They can perpetuate hidden biases, which are difficult to detect and quantify, potentially invalidating any analysis resting on their predictions.

Recent works proposed leveraging predictive models to offer valid and efficient statistical inferences on partially labeled data [Angelopoulos et al., 2023a,b], using the labeled data to adapt the model and then estimating the statistical quantities of interest using the model’s predictions on the unlabeled samples. In this paper, we focus on powering *causal inferences* on *fully unlabeled* experimental data, where an outcome of interest is captured in high-dimensional measurements such as images or videos. Together with other experimental and treatment information, the outcome predictions can be used to quantify the interventional effect of the treatment. We refer to this problem as zero-shot Prediction-Powered Causal Inference (PPCI). A key challenge is that small modeling biases can invalidate the causal conclusions, even in the simplest possible scenario, where the target experiment is a randomized controlled trial that is partially annotated [Cadei et al., 2024], so one can train on it. Still, being able to solve a PPCI problem zero-shot, i.e., without training on

the data from the target experiment, would significantly accelerate scientific discovery, for example, providing the conclusion of a new experiment in real time, without any costly and time-consuming human annotations.

To tackle this problem, we first characterize when a predictor is *valid* for a given PPCI problem. We show that (statistical) *conditional calibration* with respect to suitable experimental settings transfers the identification and estimation properties of the AIPW estimator [Robins et al., 1994] to the prediction-powered samples. This result considers an arbitrary predictor, thus opening the opportunity of training on some other *similar* experiment that shares the same outcome-measurement mechanism (i.e., concerns the same outcomes and collects the same input modality), so that it can be applied zero-shot to the new experimental data. Unfortunately, vanilla training on a similar experiment with empirical risk minimization does not guarantee valid predictors. Particularly, spurious associations between the training and target experiments may not be resolved, in some cases, even with infinite training data. To fix this, we propose *Causal Lifting*, a representation learning constraint that we show transfers causal validity under standard (yet idealized) assumptions.

Our experimental results are inspired by Cadei et al. [2024], which is to date the only real-world representation learning benchmark for treatment effect estimation. Tailoring to the discrete treatment assignments and experimental settings recorded in this benchmark, we propose a simple yet effective implementation of the causal lifting constraint via loss reweighting, which we call Deconfounded Empirical Risk Minimization (DERM). To showcase zero-shot generalization to the ISTAnt dataset, we create and release a new dataset, from our *similar* ecological experiment with a different recording platform and treatments. Remarkably, although our replica dataset is of lower quality compared to the ISTAnt experiment, we show for the first time valid PPCI on ISTAnt, which we surprisingly achieve zero-shot. We further validate and confirm the results on a synthetic manipulation of MNIST dataset [LeCun, 1998] that allows controlling for the true causal effect.

More broadly, this paper emphasizes the “representation learning” aspect of “causal representation learning” [Schölkopf et al., 2021], which has traditionally focused on the theoretical identification of a representation without concerning any specific task. In Bengio et al. [2013], good representations are defined as ones “*that make it easier to extract useful information when building classifiers or other predictors.*” In a similar spirit, we focus on representations that make extracting causal information possible with some downstream estimator. We hope that our viewpoint can also offer new benchmarking opportunities that are currently missing in the causal representation learning literature and have great potential, especially in the context of scientific discoveries.

Overall, our contributions are:

- i. a new formulation and analysis for **Prediction-Powered Causal Inference**, preserving estimation properties, motivated by real-world scientific applications,
- ii. **Causal Lifting**, a new constraint to transfer causal validity zero-shot across PPCI problems, alongside a practical implementation (DERM),
- iii. **first valid 0-shot** prediction-powered Average Treatment Effect (ATE) inference on **ISTAnt** [Cadei et al., 2024], leveraging a new dataset collected from our similar experiment.

2 Prediction-Powered Causal Inference

In this Section, we formulate the PPCI problem, introducing the terminology and general identification and estimation results characterizing a *causally* valid outcome model.

Problem: Prediction-Powered Causal Inference (PPCI)

Let $(T, W, Y, X) \sim \mathcal{P}$ be random variables, where $T \in \mathcal{T}$ denotes a treatment assignment, $W \in \mathcal{W}$ the observed covariates, $Y \in \mathcal{Y}$ the outcome of interest, and $X \in \mathcal{X}$ an high-dimensional measurement used to predict Y . Let $g : \mathcal{X} \rightarrow \mathcal{Y}$ be a fixed predictor of Y from X .

Given an i.i.d. sample $\{(T_i, W_i, X_i)\}_{i=1}^n \stackrel{i.i.d.}{\sim} \mathcal{P}$, where the outcomes are not observed directly, **identify and estimate** the average potential outcome under a treatment intervention^a, i.e., $\tau_Y(t) := \mathbb{E}[Y \mid \text{do}(T = t)]$, or related estimands, **from the prediction-powered sample** $\{(T_i, W_i, g(X_i))\}_{i \in \mathcal{I}}$.

^aWe focus on population-level causal estimands, but the problem generalizes to group-level quantities too by additionally conditioning on a covariates subset.

Several scientific problems fit under this framework, where a human domain expert, trained on similar data, acts as a predictor g , elaborating and annotating the high-dimensional measurements, aiming to collect evidence to

answer the overarching scientific question. Replacing this step with a deep learning model requires strong guarantees, which generally differ from standalone prediction accuracy metrics. Systematic errors in a specific subgroup can invalidate the full analysis, as shown in Cadei et al. [2024]. However, the PPCI potential comes from the fact that good outcome models can be learned also from similar experiments and transferred zero-shot, e.g., changing set-up and treatment of interest, as far as the (true) annotation mechanism stays invariant. Such a generalization goal is the main motivation behind the investigation of this problem, going beyond (statistical) Prediction-Powered Inference [Angelopoulos et al., 2023a,b] that is designed instead for efficiency in-distribution. As a practical, real-world motivating example, we propose to solve for the first time ATE estimation on the ISTAnt dataset zero-shot, i.e., without behaviour annotations. Instead, we leverage our own experiment variant with different treatment and recording platform, see Figure 1.

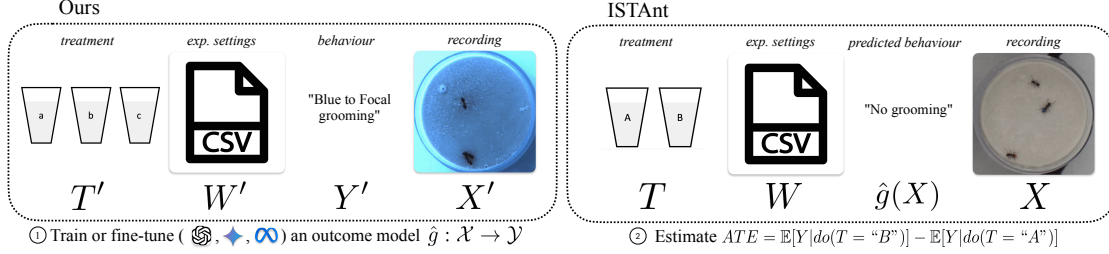


Figure 1: Illustration of our PPCI pipeline for (zero-shot) ATE estimation on ISTAnt dataset. We designed, recorded and annotated our own ISTAnt version with different treatments and recording platform and leveraged it to fine-tune a pre-trained model for imputation.

Before discussing the generalization challenges and our proposed mitigation, we formalize the properties a predictor needs to support valid PPCI and what the guarantees are. For this, note that, in the following discussion, we always start from assuming identifiability of the average potential outcome(s). Indeed, if the problem has no solution even with access to the true outcomes, the corresponding PPCI problem loses meaning.

Definition 2.1 (Valid Predictor). *An outcome predictor g is valid for a PPCI problem if and only if the average potential outcome(s) of interest $\tau_Y(t)$ identify in a statistical estimand, i.e., a treatment function removing the do-operator, and $\tau_Y(t) = \tau_{g(X)}(t)$.*

For example, given a PPCI problem \mathcal{P} with binary treatment, let the average potential outcome upon intervening on the treatment value t being identified via the adjustment formula by standard causal inference assumptions¹, i.e.,

$$\tau_Y(t) = \mathbb{E}_W[\mathbb{E}_Y[Y|T = t, W]] \quad (1)$$

where W is a valid adjustment set. A predictor g is valid for \mathcal{P} if $\tau_Y(t) = \tau_{g(X)}(t)$, i.e.,

$$\mathbb{E}_W[\mathbb{E}_Y[Y|T = t, W]] = \mathbb{E}_W[\mathbb{E}_X[g(X)|T = t, W]]. \quad (2)$$

Then, we want to characterize testable statistical property a model has to satisfy in order to be valid.

Definition 2.2 (Conditional Calibration). *Let $X, Y, Z \sim \mathcal{P}$ random variables with $X \in \mathcal{X}$ and $Y \in \mathcal{Y}$. A predictor $g : \mathcal{X} \rightarrow \mathcal{Y}$ is conditionally calibrated over Z if and only if:*

$$\mathbb{E}[Y - g(X)|Z] \stackrel{a.s.}{=} 0 \quad (3)$$

Lemma 2.1 (Prediction-Powered Identification). *Given a PPCI problem \mathcal{P} with standard causal identification assumptions. If an outcome model $g : \mathcal{X} \rightarrow \mathcal{Y}$ is conditionally calibrated with respect to the treatment and a valid adjustment set, then it is (causally) valid for \mathcal{P} .*

The lemma follows directly from backdoor adjustment (see Proof in Appendix A), and offer a sufficient condition for validity. It is worth observing that being calibrated with respect to all the observed covariates and

¹Consistency, exchangeability and overlap.

not only the valid adjustment set is just a stronger sufficient condition, still holding the thesis. For example, in experiments where there are few discrete experimental conditions, it is safe to enforce/test it for all the covariates, without requiring a prior knowledge of which is the valid adjustment set².

Lemma 2.2 (Prediction-Powered Estimation). *Given a PPCI problem \mathcal{P} with standard causal identification assumptions. If an outcome model $g : \mathcal{X} \rightarrow \mathcal{Y}$ is conditionally calibrated with respect to the treatment and a valid adjustment set, then the AIPW estimator [Robins et al., 1994] over the prediction-powered sample preserves the asymptotically valid confidence interval for the true ATE, i.e.,*

$$\sqrt{n}(\hat{\tau}_{g(X)} - \tau_Y) \rightarrow \mathcal{N}(0, V), \quad (4)$$

where V the asymptotic variance.

As before, the result is intuitive and now extend such sufficient condition to preserve the property of an estimator, i.e., asymptotic normality. The technical proof follows from classical AIPW convergence results, and we report it in Appendix A. More generally about estimation, it is important to observe that, while several estimators may exist for the same causal estimand, it is crucial to rely on a valid predictor for the statistical estimand we identify the causal one with. For example, in a randomized controlled trial, we may identify the ATE with the associational difference, and therefore require calibration only with respect to the treatment; if in practice we want to use an estimator relying on covariates conditioning to improve efficiency, e.g., AIPW, we must require the outcome model to condition on all such covariates too. We still have not discussed how to enforce or even test such a property, not having access to outcome annotations on the target experiment. For this, we need to discuss first the crucial generalization challenges in learning a valid outcome model.

2.1 Out-of-distribution generalization challenges

The main challenge in PPCI is training a valid outcome model to replace expensive and slow annotation procedures. It has to be expressive enough to process the complex input measurements, while being calibrated with respect to the experimental settings. Despite modern pre-trained models are getting more and more capable and generalist [Bubeck et al., 2024], they still cannot guarantee calibration a-priori [Chen et al., 2022]. As a human annotator learns an annotation procedure from similar experiments with the same measurement type (e.g., videos) and outcome of interest (e.g., ants behaviors), we may aim to fine-tune pre-trained models on *similar* annotated experiments, leading towards scientifically valid expert models. For this purpose, let's first provide a notion of similarity among experiments.

Definition 2.3 (Similarity). *Two PPCI problems \mathcal{P} and \mathcal{P}' are similar if their outcome-measurement mechanism is invariant, i.e.,*

$$\mathbb{P}(Y|X = x) = \mathbb{P}(Y'|X' = x) \quad \forall x \in \text{supp}(X) \cap \text{supp}(X') \quad (5)$$

This definition naturally generalizes to whatever measurement-outcome couple $(X, Y) \sim \mathcal{P}$ such that the annotation mechanism $\mathbb{P}(Y|X = x)$ is invariant. Note that our setting is different from the invariant causal predictions [Peters et al., 2016], as in our case $\mathbb{P}(Y|X = x)$ is not a causal mechanism that we want to identify using an invariance assumption over multiple environments, but rather X is a measurement of Y [Silva et al., 2006] (and thus a child of Y), potentially observed over a single environment \mathcal{P} . We can rely on this anticausal invariance whenever the same annotation protocol could be used for the two experiments (for example, humans trained to annotate \mathcal{P} are capable of annotating \mathcal{P}' without new training or instructions). Still, vanilla fine-tuning by standard empirical risk minimization over *similar* experiments doesn't guarantee learning a valid outcome model due to peculiar generalization challenges raised by the spurious shortcuts appearing in anticausal prediction problems [Schölkopf et al., 2012, Peters et al., 2016], for example, from the visual appearance of certain experimental settings. We distinguish here between statistical challenges with finite training samples and potential issues even in the infinite sample regime.

Finite training sample For a certain training subsample the model may over-rely on its spurious conditional measurement-outcome correlation, e.g., some irrelevant background information. If on target the measurements in such subgroup are over-representing a certain treatment value or other outcome's ancestors, it may invalidate any causal downstream prediction-powered estimation.

²Note that the requirements here are different than covariate adjustment, and calibrating only to a minimal set is not necessary if the model can be practically calibrated on more variables without losing predictive performances.

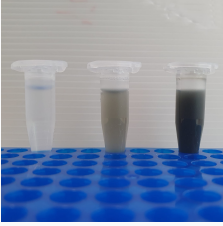
Example 1: Background confounding


Consider PPCI within the ISTant dataset, annotating a first batch of videos for training. If a certain behaviour is underrepresented in a specific plate, e.g., because the plate is in the control group, the model can leverage such spurious shortcut in subsequent batches, relying on background information like the pen markings on the floor to identify the plate. This invalidates any downstream prediction-powered analysis, as future plates may be treated, but the model may assume they are not, matching the target statistics with the control group.

Infinite training sample Additionally, treatment information captured in the measurement that is not mediated by the outcome may be misleading for generalization, even in the infinite training sample setting. In other words, a double blind experiment needs to be blind also for the model, which should not be able to guess the treatment if not through the effect. Otherwise, prior correlations between other treatments and the effect can propagate to the new experiment. For example, say a model was trained on an experiment using treatment $T' = t'$. In the target experiment, we consider a different treatment $T = t$ that “looks like t' ”, i.e., given an image that may come from either experiment, t and t' are equally likely:

$$\mathbb{P}(T = t | X = x) = \mathbb{P}(T' = t' | X' = x) \quad \forall x \in \text{supp}(X) \cap \text{supp}(X'). \quad (6)$$

The model, that is only trained on t' and has never seen t during training, may introduce correlations with the training treatment effect. For example, if an outcome value never happens in the training treatment ($\text{supp}(Y' | T' = t') \subset \text{supp}(Y')$), the model will wrongly transfer this to the target population, invalidating any causal downstream prediction-powered estimation. The same argument also holds replacing the treatment with any other outcome’s ancestor.

Example 2: Different treatments with similar appearance


Consider two experiments where the treatments are visually similar, discernible from the control, and differing in the effect, e.g., different pathogen suspension exposure with liquid residual in the measurements. While learning, an outcome model may over-rely on the training treatment effect, e.g., excluding the possibility of a specific behaviour, and wrongly transfer during PPCI on the target experiment. Note that this is not the case for our experiment and ISTant where the treatment is not visible, as for well-designed double blind experiments.

3 Causal Lifting of Neural Representations

In the previous Section we presented and discussed the PPCI problem and its peculiar challenges to learn a valid outcome model. In this Section, we introduce a new representation learning constraint to prevent such generalization challenges, and corresponding implementation, tailored for our application of interest.

Definition 3.1 (Causal Lifting constraint). *Given a PPCI problem \mathcal{P} with standard causal identification assumptions, and a predictor $g = h \circ \phi : \mathcal{X} \rightarrow \mathcal{Y}$. The encoder $\phi : \mathcal{X} \rightarrow \mathbb{R}^d$ satisfies the Causal Lifting constraint when:*

$$I(\phi(X), Z | Y) = 0, \quad (7)$$

where $Z = [T, \tilde{W}]$, and $\tilde{W} \subseteq W$ is a valid adjustment set.

The Causal Lifting constraint is a condition on the model encoder to prevent the possibility to leverage unnecessary spurious outcome information from the experimental settings.

Theorem 3.1 (Causal Lifting transfers causal validity). *Given two similar PPCI problems \mathcal{P} and \mathcal{P}' with standard causal identification assumptions. Let $g = h \circ \phi : \mathcal{X} \rightarrow \mathcal{Y}$ be an outcome model for \mathcal{P}' with h Bayes-optimal, and assume that the representation transfers, i.e., $\mathbb{P}(\phi(X) | Y) = \mathbb{P}'(\phi(X) | Y)$. Then the Causal Lifting constraint on \mathcal{P} implies g is valid on \mathcal{P} .*

Theorem 3.1 offers a sufficient condition to transfer model validity from a training experiment to a target experiment by assuming the Causal Lifting constraint holding on target. It combines the strengths of modern

deep learning models, able to extract sufficient representations on training tasks, i.e., $I(Y|\phi(X)) = I(Y|X)$, together with efficient fitting on limited data, i.e., Bayes Optimal classifier assumption. We remark that the assumption that the representation transfers is reasonable, since we have assumed that an invariant annotation protocol exists. In practice, the Causal Lifting constraint is required to hold on the target experiment, where we cannot get any guarantees without labels. However, referring to the generalization challenges examples in Section 2:

- in Example 1, the causal lifting constraint prevents the outcome model to leverage the spurious shortcuts from the background information by enforcing it to be position independent, i.e., background-agnostic,
- in Example 2, it prevents the outcome model to leverage the spurious training treatment effect information, by enforcing it to be treatment agnostic.

Despite the unverifiability of this assumption, we practically rely on the hope that transferring such property is an easier generalization task than transferring conditional calibration. We then propose to enforce the causal lifting constraint during training/fine-tuning *on the treatment and the valid adjustment set for the target experiment*, when also observed. If not observed but constant in the training experiment, the condition is satisfied by default (no signal for the model to learn such experimental settings). As pre-trained models trained on huge generic data are very capable of detecting all visible information that can correlate with a prediction target, the causal-lifting constraint has to be enforced explicitly during transfer learning, forcing the artificial annotation process to be “blind”. Similar to the Conditional Calibration assumption, if the outcome is predictable well from the measurement, enforcing the causal lifting constraint on more experimental settings than necessary does not hurt.

3.1 Deconfounded Empirical Risk Minimization

The Causal Lifting constraint is a conditional independence condition, and as such, enforcing it during training is a well-known problem in the Representation Learning literature. Different direct and indirect approaches have already been proposed, and in Section 4 we overview the major paradigms. Here, we propose a simple implementation that is tailored to common assumptions in scientific experiments (and that are true in ISTAnt), i.e., that experimental settings are low-dimensional and discrete [Pearl et al., 2000, Rosenbaum et al., 2010]. Other more general implementations are certainly possible if such assumptions do not hold, but this is beyond the scope of this paper. In detail, we leverage a resampling approach [Kirichenko et al., 2022, Li and Vasconcelos, 2019], reweighting the training distribution to simulate a distribution that has no correlation between outcome and experimental settings, while keeping the annotation mechanism invariant. We define the manipulated distribution of Z^*, Y^* as function of Z, Y and joint distribution:

$$\mathbb{P}(Y^* = y, Z^* = z) := \begin{cases} 0 & \text{if } |\text{supp}(Y|Z = z)| = 0 \\ \frac{\mathbb{P}(Y^*|Z^*=z)}{1} \cdot \frac{\mathbb{P}(Z^*=z)}{\sum_{z' \in \mathcal{Z}} \text{Var}(Y|Z = z')} & \text{otherwise} \end{cases} \quad (8)$$

for all $y \in \mathcal{Y}, z \in \mathcal{Z}$, where $\text{supp}(Y|Z = z) = \{y \in \mathcal{Y} : \mathbb{P}(Y = y|Z = z) > 0\}$. By design such joint distribution depends only on the experimental settings values, i.e., the conditional outcome distribution $\mathbb{P}(Y^*|Z^* = z)$ is uniform, while the experimental settings marginal $\mathbb{P}(Z^* = z)$ weights more the observations with the least outcome-informative experimental settings (high conditional variance) over the training population, and ignores the most informative ones (low or null variance).

If the conditional outcome support is full for each not fully informative covariates value, i.e.,

$$\text{supp}(Y|Z = z) = \text{supp}(Y) \quad \forall z \in \mathcal{Z} : \text{Var}(Y|Z = z) > 0, \quad (9)$$

then, the conditional outcome distribution is constant and $Y^* \perp\!\!\!\perp Z^*$. It follows that an outcome model trained on such distribution has no signal from the outcome to learn the uncorrelated experimental settings, naturally enforcing the Causal Lifting constraint.

We then propose to train/fine-tune the factual outcome model minimizing the empirical risk, e.g., via Stochastic Gradient Descent, on such ‘disentangled’ distribution reweighting each observation i by a factor:

$$w_i = \frac{\hat{\mathbb{P}}(Y^* = y, Z^* = z)}{\hat{\mathbb{P}}(Y = y, Z = z)}, \quad (10)$$

computed *una-tantum* before starting the training, estimating the joint training distribution by frequency (denominator), and the conditional variances by sample variance (nominator). We refer to this procedure as *Deconfounded Empirical Risk Minimization* (DERM).

Finally, we remark that when Condition 9 doesn’t hold, it is not possible to specify a ‘disentangled’ joint distribution without ignoring the experimental settings, i.e., $\mathbb{P}(Z^* = z) = 0$, where the conditional outcome’s support is strictly contained in the marginal outcome’s support on the training distribution. Our manipulated distribution will still consider these samples, but reducing their weight with respect to the predictivity of the observed experimental setting (approximately $\propto \text{Var}(Y|Z = z)$). Therefore, some spurious correlations may still be learned, but this is now in a trade-off with ignoring a potentially substantial part of the reference sample. While this does not apply to our application of interest, tailored modifications of our joint distribution can be proposed case-by-case.

4 Related Works

Prediction-Powered Causal Inference The factual outcome estimation problem for causal inference from high-dimensional observations was first introduced by Cadei et al. [2024]. We extended the problem to generalization from similar experiments, motivated by practical desiderata, e.g., in experimental ecology. In our paper, we formalize what they describe as “encoder bias”, and our DERM is the first proposal to their call for “*new methodologies to mitigate this bias during adaptation*”, although we consider an additional OOD component. Demirel et al. [2024], Wang et al. [2024] already attempted to discuss some generalization challenges in a PPCI problem, but with unrealistic assumptions. They ignored any high-dimensional measurement of the outcome of interest and assumed that the experimental settings alone are sufficient for factual outcome estimation together with support overlapping, i.e., without generalization, making the model too application-specific and ignoring any connection with representation learning. Let’s further observe that their framework is a special case of ours when X is low-dimensional, and the target experiment is in-distribution. In contrast to the classic Prediction-Powered Inference (PPI) [Angelopoulos et al., 2023a,b], which improves estimation efficiency by imputing unlabeled in-distribution data via a predictive model, and recent causal inference extensions [Wang et al., 2024, De Bartolomeis et al., 2025, Poulet et al., 2025] relying on counterfactual predictions, PPCI focuses on imputing missing *factual* outcomes to generalize across similar experiments.

Invariant representations Learning representations invariant to certain attributes is a widely studied problem in machine learning [Moyer et al., 2018, Arjovsky et al., 2019, Gulrajani and Lopez-Paz, 2021, Krueger et al., 2021, Yao et al., 2024a]. In some sense, we wish to learn representations of X that can predict the outcome Y , but are invariant to the experimental variables Z . In agreement with Yao et al. [2024a], we combine a sufficiency objective with our causal lifting constraint in the representation space, enforcing a suitable representation invariance. Several alternative approaches can be considered to enforce such conditional independence constraints: (i) Conditional Mutual Information Minimization [Song et al., 2019, Cheng et al., 2020, Gupta et al., 2021], (ii) Adversarial Independence Regularization such as Louizos et al. [2015] which modifies variational autoencoder (VAE) architecture in Kingma [2014] to learn *fair* representations that are invariant sensitive attributes, by training against an adversary that tries to predict those variables, (iii) Conditional Contrastive Learning such as Ma et al. [2021] whereby one learns representations invariant to certain attributes by optimizing a conditional contrastive loss, (iv) Variational Information Bottleneck methods where one learns useful and sufficient representations invariant to a specific *domain* [Aleml et al., 2016, Li et al., 2022]. We chose our DERM procedure as it matches well our application of interest, but other applications may prefer different conditional independence implementations.

Causal Representation Learning In the broader context of causal representation learning methods [Schölkopf et al., 2021], our proposal largely focuses on representation learning applications to causal inference: learning representations of data that make it possible to estimate causal estimands. We find it in contrast with most recent works in causal representation learning, which uniquely focused on complete identifiability of all the variables or blocks, see Varici et al. [2024], von Kügelgen [2024] for recent overviews targeting general settings. The main exceptions are Yao et al. [2024a,b]. The former leverages domain generalization regularizers to debias treatment effect estimation in ISTAnt from selection bias. However, their proposal is not sufficient to prevent confounding when no data from the target experiment is given. The latter uses multi-view causal representation learning models to model confounding for adjustment in an observational climate application. In our paper, we also discuss conditions for identification, but we focus on a specific causal estimand, as opposed to block-identifiability of causal variables. As opposed to virtually

all existing work in causal representation learning, our perspective offers clear evaluation and benchmarking potential on *real world* scientific experiments – even in theoretically under-specified settings via the accuracy of the causal estimate.

5 Experiments

In pursuit of scientific validity, we evaluate our method (DERM) on the ISTAnt dataset [Cadei et al., 2024], and additional synthetic experiments controlling for the true causal effect.

Zero-Shot Generalization on ISTAnt. We performed a *similar* experiment to the ISTAnt experiment on our recording platform, considering three different treatments and collecting 44 annotated 30-minute videos, and we leveraged such annotated videos to fine-tune a pretrained model generalizing zero-shot prediction powered ATE inference on ISTAnt by AIPW. We considered the AIPW estimation on the (true) ISTAnt human annotated outcomes as the ground truth ATE (approximately +40s in grooming time per video). Further details on the modeling choices, hyper-parameter, and fine-tuning are discussed in Appendix B. Figure 3 shows the differences in filming setup among the two experiments.

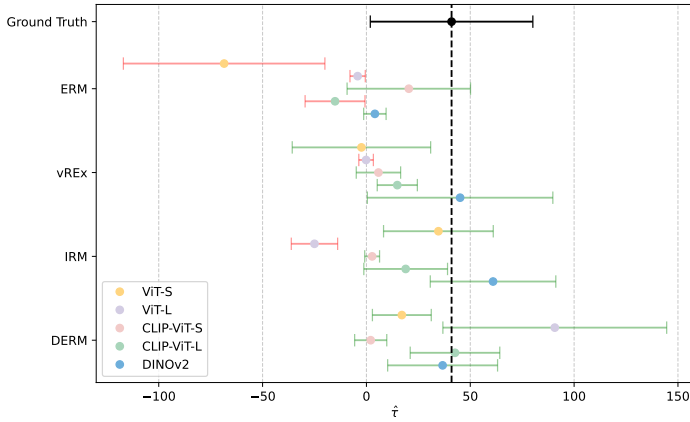


Figure 2: 0-shot PP-ATE inference on ISTAnt dataset from our similar experiment, varying method and pre-trained encoder. Reported the 95% confidence intervals estimated via AIPW asymptotic normality and compared against the same inference on the annotated outcomes. In green the correct confidence intervals (overlapping 33+%) in red the incorrect.

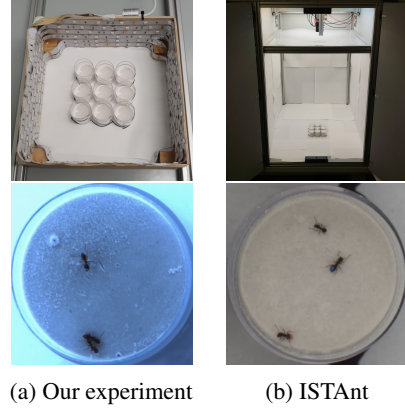


Figure 3: Filming box and example frame from our experiment and ISTAnt. The two experiments mainly differ in lighting conditions, treatments, experimental nests (wall height) and color marking.

Figure 2 reports the ATE estimation 95% confidence intervals per method-encoder (five different pre-trained backbones) by AIPW asymptotic normality, selecting per group the model across minimizing the treatment effect bias on reference. We trained multiple nonlinear heads, i.e., multi-layer perceptron, on top via (i) vanilla ERM, (ii) Variance Risk Extrapolation (vREx) Krueger et al. [2021], (iii) Invariance Risk Minimization Arjovsky et al. [2019] (IRM) and (iv) DERM (ours). As expected, fine-tuning via vanilla ERM leads to consistently underestimating/ignoring the effect (no validity guarantees). IRM and vREx, as proposed by Yao et al. [2024a], performs better, despite still being occasionally invalid. DERM is the only method consistently providing valid ATE inference for all the pre-trained models, without ever estimating the effect with the wrong sign, unlike ERM, vREx and IRM.

CausalMNIST. We replicate the analysis on a colored manipulations of the MNIST dataset, e.g., estimating the effect of the background color or pen color on the digit value, allowing complete control of the causal effects and uncertainty quantification by Monte Carlo simulations. We train a convolutional neural network on an experiment and we test zero-shot PPCI on four similar observational studies, varying the treatment effect mechanism and experimental settings distribution, challenging the full support assumption, i.e., Equation 9. A full description of the data-generating processes and analysis is reported in Appendix C.

The results are reported in Table 1, clearly showing the DERM potential to solve unsolvable instances for both ERM and invariant training (see soft shifts columns), while suffering when challenging its assumptions (see hard shifts columns).

Table 1: Zero-shot PPCI results on CausalMNIST varying the target experiment population (in-, out-of-distribution), the treatment effect mechanism (linear, non-linear) and challenging the full-support guarantees (soft, hard shifts). We report the ATE estimation bias and standard deviation over 50 repetitions.

Method	In-Distribution	OoD (<i>linear effect</i>)		OoD (<i>non-linear effect</i>)	
		Soft shift	Hard shift	Soft shift	Hard shift
Ground Truth ³	0.00 ± 0.02	0.00 ± 0.02	0.00 ± 0.02	0.04 ± 0.05	0.03 ± 0.05
ERM	0.00 ± 0.02	0.86 ± 0.14	1.05 ± 0.15	0.64 ± 0.18	0.85 ± 0.17
vREx	0.01 ± 0.03	0.83 ± 0.15	1.05 ± 0.14	0.55 ± 0.17	0.82 ± 0.14
IRM	0.01 ± 0.03	0.76 ± 0.18	1.02 ± 0.12	0.45 ± 0.18	0.77 ± 0.17
DERM (ours)	0.10 ± 0.07	0.14 ± 0.14	0.75 ± 0.05	0.08 ± 0.27	0.45 ± 0.12

6 Conclusion

In this paper, we introduced the challenge of solving PPCI problems zero-shot. We are motivated by scientific applications, where predictors can be trained on existing data collected in prior experiments and power valid causal conclusions in new experiments without further training. Theoretically, we developed the first identification and estimation results for PPCI, alongside a causal lifting constraint that transfers causal validity under standard yet idealized assumptions. In practice, we have offered an implementation of the causal lifting constraint with our Deconfounded Empirical Risk Minimization, and showed that it achieves zero-shot identification of the ATE on the ISTAnt dataset [Cadei et al., 2024] by leveraging (our) *similar* ecological experiment. Overall, our work offers a paradigm shift from the traditional causal representation learning literature [Schölkopf et al., 2021], paving the way toward learning representations that power downstream causal estimates on real-world data. We think that this has the potential to play a critical role for deep learning models to accelerate the analysis of scientific data and ultimately new discoveries.

The main limitation of this work is that, in practice, it is not possible to verify whether either the conditional calibration property or the causal lifting constraint actually holds on the target population without annotations. Beyond our key assumption that the representation transfers, we also did not discuss the model convergence on finite training datasets, so even if enforcing the causal lifting on training would transfer, we may still suffer from finite sample effects. Another limitation is neglecting several settings that are, potentially, practically relevant, e.g., not overlapping effect modifiers among similar experiments, or the violation of Condition 9. As our target experiments did not have these problems, we left them for future work. Finally, we rest on the assumption that the underlying causal inference problem is statistically identifiable, but this is necessary and can be ensured with a well-designed experimental protocol. Despite these limitations, we hope our work can inspire a new generation of practical causal representation learning methodologies and create opportunities for more systematic and practically relevant benchmarking.

Acknowledgments

We thank the Causal Learning and Artificial Intelligence group at ISTA for the continuous feedback on the project and valuable discussions. We thank the Social Immunity group at ISTA, particularly Jinook Oh, for the annotation program and Michaela Hoenigsberger for supporting our ecological experiment. Riccardo Cadei is supported by a Google Research Scholar Award and a Google Initiated Gift to Francesco Locatello. This research was funded in part by the Austrian Science Fund (FWF) 10.55776/COE12). It was further in part supported by the ISTA Interdisciplinary Project Committee for the collaborative project “ALED” between Francesco Locatello and Sylvia Cremer. For open access purposes, the author has applied a CC BY public copyright license to any author accepted manuscript version arising from this submission.

³By AIPW asymptotic normality on the true factual outcomes.

References

- John Jumper, Richard Evans, Alexander Pritzel, Tim Green, Michael Figurnov, Olaf Ronneberger, Kathryn Tunyasuvunakool, Russ Bates, Augustin Žídek, Anna Potapenko, et al. Highly accurate protein structure prediction with alphafold. *nature*, 596(7873):583–589, 2021.
- Kathryn Tunyasuvunakool, Jonas Adler, Zachary Wu, Tim Green, Michal Zielinski, Augustin Žídek, Alex Bridgland, Andrew Cowie, Clemens Meyer, Agata Laydon, et al. Highly accurate protein structure prediction for the human proteome. *Nature*, 596(7873):590–596, 2021.
- Haitham A Elmarakeby, Justin Hwang, Rand Arafeh, Jett Crowdis, Sydney Gang, David Liu, Saud H AlDubayan, Keyan Salari, Steven Kregel, Camden Richter, et al. Biologically informed deep neural network for prostate cancer discovery. *Nature*, 598(7880):348–352, 2021.
- Michael W Mullowney, Katherine R Duncan, Somayah S Elsayed, Neha Garg, Justin JJ van der Hooft, Nathaniel I Martin, David Meijer, Barbara R Terlouw, Friederike Biermann, Kai Blin, et al. Artificial intelligence for natural product drug discovery. *Nature Reviews Drug Discovery*, 22(11):895–916, 2023.
- Miao Zhong, Kevin Tran, Yimeng Min, Chuanhao Wang, Ziyun Wang, Cao-Thang Dinh, Phil De Luna, Zongqian Yu, Armin Sedighian Rasouli, Peter Brodersen, et al. Accelerated discovery of co2 electrocatalysts using active machine learning. *Nature*, 581(7807):178–183, 2020.
- David Rolnick, Priya L Donti, Lynn H Kaack, Kelly Kochanski, Alexandre Lacoste, Kris Sankaran, Andrew Slavin Ross, Nikola Milojevic-Dupont, Natasha Jaques, Anna Waldman-Brown, et al. Tackling climate change with machine learning. *ACM Computing Surveys (CSUR)*, 55(2):1–96, 2022.
- Connor T Jerzak, Fredrik Johansson, and Adel Daoud. Image-based treatment effect heterogeneity. *arXiv preprint arXiv:2206.06417*, 2022.
- Adel Daoud, Felipe Jordán, Makkunda Sharma, Fredrik Johansson, Devdatt Dubhashi, Sourabh Paul, and Subhashis Banerjee. Using satellite images and deep learning to measure health and living standards in india. *Social Indicators Research*, 167(1):475–505, 2023.
- Anastasios N Angelopoulos, Stephen Bates, Clara Fannjiang, Michael I Jordan, and Tijana Zrnica. Prediction-powered inference. *Science*, 382(6671):669–674, 2023a.
- Anastasios N Angelopoulos, John C Duchi, and Tijana Zrnica. Ppi++: Efficient prediction-powered inference. *arXiv preprint arXiv:2311.01453*, 2023b.
- Riccardo Cadei, Lukas Lindorfer, Sylvia Cremer, Cordelia Schmid, and Francesco Locatello. Smoke and mirrors in causal downstream tasks. *arXiv preprint arXiv:2405.17151*, 2024.
- James Robins, Andrea Rotnitzky, and Lue Ping Zhao. Estimation of regression coefficients when some regressors are not always observed. *Journal of the American statistical Association*, 89(427):846–866, 1994.
- Yann LeCun. The mnist database of handwritten digits. <http://yann.lecun.com/exdb/mnist/>, 1998.
- Bernhard Schölkopf, Francesco Locatello, Stefan Bauer, Nan Rosemary Ke, Nal Kalchbrenner, Anirudh Goyal, and Yoshua Bengio. Toward causal representation learning. *Proceedings of the IEEE*, 109(5):612–634, 2021.
- Yoshua Bengio, Aaron Courville, and Pascal Vincent. Representation learning: A review and new perspectives. *IEEE transactions on pattern analysis and machine intelligence*, 35(8):1798–1828, 2013.
- Sébastien Bubeck, Varun Chandrasekaran, Ronen Eldan, Johannes Gehrke, Eric Horvitz, Ece Kamar, Peter Lee, Yin Tat Lee, Yuanzhi Li, Scott Lundberg, et al. Sparks of artificial general intelligence: Early experiments with gpt-4. arxiv 2023. *arXiv preprint arXiv:2303.12712*, 10, 2024.
- Yangyi Chen, Lifan Yuan, Ganqu Cui, Zhiyuan Liu, and Heng Ji. A close look into the calibration of pre-trained language models. *arXiv preprint arXiv:2211.00151*, 2022.
- Jonas Peters, Peter Bühlmann, and Nicolai Meinshausen. Causal inference by using invariant prediction: identification and confidence intervals. *Journal of the Royal Statistical Society Series B: Statistical Methodology*, 78(5):947–1012, 2016.
- Ricardo Silva, Richard Scheines, Clark Glymour, Peter Spirtes, and David Maxwell Chickering. Learning the structure of linear latent variable models. *Journal of Machine Learning Research*, 7(2), 2006.
- Bernhard Schölkopf, Dominik Janzing, Jonas Peters, Eleni Sgouritsa, Kun Zhang, and Joris Mooij. On causal and anticausal learning. In *Proceedings of the 29th International Conference on International Conference on Machine Learning*, pages 459–466, 2012.

- Judea Pearl et al. Models, reasoning and inference. *Cambridge, UK: CambridgeUniversityPress*, 19(2):3, 2000.
- Paul R Rosenbaum, P Rosenbaum, and Briskman. *Design of observational studies*, volume 10. Springer, 2010.
- Polina Kirichenko, Pavel Izmailov, and Andrew Gordon Wilson. Last layer re-training is sufficient for robustness to spurious correlations. *arXiv preprint arXiv:2204.02937*, 2022.
- Yi Li and Nuno Vasconcelos. Repair: Removing representation bias by dataset resampling. In *Proceedings of the IEEE/CVF conference on computer vision and pattern recognition*, pages 9572–9581, 2019.
- Ilker Demirel, Ahmed Alaa, Anthony Philippakis, and David Sontag. Prediction-powered generalization of causal inferences. *arXiv preprint arXiv:2406.02873*, 2024.
- Yuxin Wang, Maresa Schröder, Dennis Frauen, Jonas Schweisthal, Konstantin Hess, and Stefan Feuerriegel. Constructing confidence intervals for average treatment effects from multiple datasets. *arXiv preprint arXiv:2412.11511*, 2024.
- Piersilvio De Bartolomeis, Javier Abad, Guanbo Wang, Konstantin Donhauser, Raymond M. Duch, Fanny Yang, and Issa J. Dahabreh. Efficient randomized experiments using foundation models. *arXiv preprint arxiv:2502.04262*, 2025.
- Pierre-Emmanuel Poulet, Maylis Tran, Sophie Tezenas du Montcel, Bruno Dubois, Stanley Durrleman, and Bruno Jedynak. Prediction-powered inference for clinical trials. *medRxiv*, pages 2025–01, 2025.
- Daniel Moyer, Shuyang Gao, Rob Brekelmans, Aram Galstyan, and Greg Ver Steeg. Invariant representations without adversarial training. *Advances in neural information processing systems*, 31, 2018.
- Martin Arjovsky, Léon Bottou, Ishaan Gulrajani, and David Lopez-Paz. Invariant risk minimization. *arXiv preprint arXiv:1907.02893*, 2019.
- Ishaan Gulrajani and David Lopez-Paz. In search of lost domain generalization. In *International Conference on Learning Representations*, 2021.
- David Krueger, Ethan Caballero, Joern-Henrik Jacobsen, Amy Zhang, Jonathan Binas, Dinghui Zhang, Remi Le Priol, and Aaron Courville. Out-of-distribution generalization via risk extrapolation (rex). In *International conference on machine learning*, pages 5815–5826. PMLR, 2021.
- Dingling Yao, Dario Rancati, Riccardo Cadei, Marco Fumero, and Francesco Locatello. Unifying causal representation learning with the invariance principle. *arXiv preprint arXiv:2409.02772*, 2024a.
- Jiaming Song, Pratyusha Kalluri, Aditya Grover, Shengjia Zhao, and Stefano Ermon. Learning controllable fair representations. In *The 22nd International Conference on Artificial Intelligence and Statistics*, pages 2164–2173. PMLR, 2019.
- Pengyu Cheng, Weituo Hao, Shuyang Dai, Jiachang Liu, Zhe Gan, and Lawrence Carin. Club: A contrastive log-ratio upper bound of mutual information. In *International conference on machine learning*, pages 1779–1788. PMLR, 2020.
- Umang Gupta, Aaron M Ferber, Bistra Dilkina, and Greg Ver Steeg. Controllable guarantees for fair outcomes via contrastive information estimation. In *Proceedings of the AAAI Conference on Artificial Intelligence*, volume 35-9, pages 7610–7619, 2021.
- Christos Louizos, Kevin Swersky, Yujia Li, Max Welling, and Richard Zemel. The variational fair autoencoder. *arXiv preprint arXiv:1511.00830*, 2015.
- Diederik P Kingma. Adam: A method for stochastic optimization. *arXiv preprint arXiv:1412.6980*, 2014.
- Martin Q Ma, Yao-Hung Hubert Tsai, Paul Pu Liang, Han Zhao, Kun Zhang, Ruslan Salakhutdinov, and Louis-Philippe Morency. Conditional contrastive learning for improving fairness in self-supervised learning. *arXiv preprint arXiv:2106.02866*, 2021.
- Alexander A Alemi, Ian Fischer, Joshua V Dillon, and Kevin Murphy. Deep variational information bottleneck. *arXiv preprint arXiv:1612.00410*, 2016.
- Bo Li, Yifei Shen, Yezhen Wang, Wenzhen Zhu, Dongsheng Li, Kurt Keutzer, and Han Zhao. Invariant information bottleneck for domain generalization. In *Proceedings of the AAAI Conference on Artificial Intelligence*, volume 36-7, pages 7399–7407, 2022.
- Burak Varici, Emre Acartürk, Karthikeyan Shanmugam, and Ali Tajer. General identifiability and achievability for causal representation learning. In *International Conference on Artificial Intelligence and Statistics*, pages 2314–2322. PMLR, 2024.

- Julius von Kügelgen. *Identifiable Causal Representation Learning: Unsupervised, Multi-View, and Multi-Environment*. PhD thesis, Cambridge University, 2024.
- Dingling Yao, Caroline Muller, and Francesco Locatello. Marrying causal representation learning with dynamical systems for science. *Advances in Neural Information Processing Systems (NeurIPS)*, 2024b.
- Donald B Rubin. Estimating causal effects of treatments in randomized and nonrandomized studies. *Journal of educational Psychology*, 66(5):688, 1974.
- Edward H Kennedy, Sivaraman Balakrishnan, and Max G’sell. Sharp instruments for classifying compliers and generalizing causal effects. 2020.
- Alexey Dosovitskiy, Lucas Beyer, Alexander Kolesnikov, Dirk Weissenborn, Xiaohua Zhai, Thomas Unterthiner, Mostafa Dehghani, Matthias Minderer, Georg Heigold, Sylvain Gelly, et al. An image is worth 16x16 words: Transformers for image recognition at scale. *arXiv preprint arXiv:2010.11929*, 2020.
- Xiaohua Zhai, Basil Mustafa, Alexander Kolesnikov, and Lucas Beyer. Sigmoid loss for language image pre-training. In *Proceedings of the IEEE/CVF International Conference on Computer Vision*, pages 11975–11986, 2023.
- Alec Radford, Jong Wook Kim, Chris Hallacy, Aditya Ramesh, Gabriel Goh, Sandhini Agarwal, Girish Sastry, Amanda Askell, Pamela Mishkin, Jack Clark, et al. Learning transferable visual models from natural language supervision. In *International conference on machine learning*, pages 8748–8763. PMLR, 2021.
- Maxime Oquab, Timothée Darcet, Théo Moutakanni, Huy Vo, Marc Szafraniec, Vasil Khalidov, Pierre Fernandez, Daniel Haziza, Francisco Massa, Alaaeldin El-Nouby, et al. Dinov2: Learning robust visual features without supervision. *arXiv preprint arXiv:2304.07193*, 2023.

Appendix

Table of Contents

A Proofs	13
A.1 Proof of Lemma 2.1	13
A.2 Proof of Lemma 2.2	14
A.3 Proof of Theorem 3.1	16
B ISTAnt	17
B.1 Similar experiment and data recording (ours)	17
B.2 Zero-shot PPCI	17
C CausalMNIST	19
C.1 Data Generating Process	19
C.2 Analysis	20

A Proofs

Note: In the rest of the manuscript we use the expression "under standard causal identification assumptions" to refer to the canonical conditions for identifiability in a observational study (and so a randomized controlled trial too) [Rubin, 1974], i.e.,:

- *Stable Unit Treatment Value Assumption (SUTVA)*, i.e., not interference and no hidden version of the treatment,
- *Overlap Assumption*, i.e., $0 < \mathbb{E}[T|W = w] < 1$ for all $w \in \mathcal{W}$,
- *Conditional Exchangeability (or Unconfoundness) Assumption*, i.e., $\mathbb{P}(Y|do(T = t), W) = \mathbb{P}(Y|T = t, W)^4$.

A.1 Proof of Lemma 2.1

Lemma (Prediction-Powered Identification). *Given a PPCI problem \mathcal{P} with standard causal identification assumptions. If an outcome model $g : \mathcal{X} \rightarrow \mathcal{Y}$ is conditionally calibrated with respect to the treatment and a valid adjustment set, then it is (causally) valid for \mathcal{P} .*

Proof. Given the identification of the causal estimand, the thesis follows directly by the tower rule over a valid adjustment set \tilde{W} and leveraging the conditional calibration:

$$\tau_Y(t) = \mathbb{E}[Y|do(T = t)] = \quad (11)$$

$$= \mathbb{E}_{\tilde{W}}[\mathbb{E}_Y[Y|do(T = t), \tilde{W}]] = \quad (12)$$

$$= \mathbb{E}_{\tilde{W}}[\mathbb{E}_Y[Y|T = t, \tilde{W}]] = \quad (13)$$

$$= \mathbb{E}_{\tilde{W}}[\mathbb{E}_X[g(X)|T = t, \tilde{W}]] = \tau_{g(X)}(t) \quad \forall t \in \mathcal{T}. \quad (14)$$

□

⁴Re-framing it in *do*-calculus notation.

A.2 Proof of Lemma 2.2

Lemma (Prediction-Powered Estimation). *Given a PPCI problem \mathcal{P} with standard causal identification assumptions. If an outcome model $g : \mathcal{X} \rightarrow \mathcal{Y}$ is conditionally calibrated with respect to the treatment and a valid adjustment set, then the AIPW estimator [Robins et al., 1994] over the prediction-powered sample with nuisance function estimators satisfying $\|\hat{\mu} - \mu\| \cdot \|\hat{e} - e\| = o_{\mathbb{P}}(n^{-1/2})$, preserves the asymptotically valid confidence interval for the true ATE, i.e.,*

$$\sqrt{n}(\hat{\tau}_{g(X)} - \tau_Y) \rightarrow \mathcal{N}(0, V),$$

where V the asymptotic variance.

Proof. Our goal is to prove that the following estimator for τ_Y is asymptotically normal:

$$\hat{\tau}_{g(X)} = \frac{1}{n} \sum_{i=1}^n \left[\hat{\mu}_{g(X)}(W_i, 1) - \hat{\mu}_{g(X)}(W_i, 0) + \frac{T_i}{\hat{e}(W_i)}(g(X_i) - \hat{\mu}_{g(X)}(W_i, 1)) - \frac{1 - T_i}{1 - \hat{e}(W_i)}(g(X_i) - \hat{\mu}_{g(X)}(W_i, 0)) \right] \quad (15)$$

where $\hat{\mu}_{g(X)}(w, t)$ is an estimator of the true predicted-outcome model $\mu_{g(X)}(w, t) = \mathbb{E}[g(X)|W = w, T = t]$, and $\hat{e}(w)$ is an estimator of the true propensity score $e(w) = \mathbb{P}(T = 1|W = w)$.

Given a generic outcome model μ and a propensity score e , let us define the influence function of the estimator:

$$\phi(O_i; \mu, e, g) = \mu(W_i, 1) - \mu(W_i, 0) + \frac{T_i}{e(W_i)}(g(X_i) - \mu(W_i, 1)) - \frac{1 - T_i}{1 - e(W_i)}(g(X_i) - \mu(W_i, 0)), \quad (16)$$

where $O_i = (T_i, W_i, Y_i, X_i)$. Then

$$\hat{\tau}_{g(X)} = \frac{1}{n} \sum_{i=1}^n \phi(O_i; \hat{\mu}_{g(X)}, \hat{e}, g). \quad (17)$$

We can rewrite our estimator as:

$$\hat{\tau}_{g(X)} - \tau_Y = \frac{1}{n} \sum_{i=1}^n [\phi(O_i; \mu, e, g) - \tau_Y] + \frac{1}{n} \sum_{i=1}^n \underbrace{[\phi(O_i; \hat{\mu}_{g(X)}, \hat{e}, g) - \phi(O_i; \mu, e, g)]}_{\Delta_i}, \quad (18)$$

where $\mu(w, t) = \mathbb{E}[Y|W = w, T = t]$ is the true outcome model and by conditional calibration:

$$\mu(w, t) = \mathbb{E}[Y|W = w, T = t] = \mathbb{E}[g(X)|W = w, T = t] \quad \forall w \in \mathcal{W}, t \in \mathcal{T}. \quad (19)$$

Assuming that the second moment of the random variable ϕ is bounded, by a standard central limit theorem argument, the first term satisfies

$$\sqrt{n} \left(\frac{1}{n} \sum_{i=1}^n \phi(O_i; \mu, e, g) - \tau_Y \right) \xrightarrow{d} \mathcal{N}(0, \underbrace{\mathbb{E}[\phi^2]}_V). \quad (20)$$

It remains to show that the second term multiplied by \sqrt{n} goes to zero in probability, i.e. it is asymptotically negligible. To do so, observe that we can rewrite the second term as

$$\frac{1}{n} \sum_{i=1}^n \Delta_i = (\mathbb{P}_n - \mathbb{P})(\Delta_i) + \mathbb{P}(\Delta_i), \quad (21)$$

where \mathbb{P} and \mathbb{P}_n are the true and empirical target measures; $\mathbb{P}(\cdot) = \mathbb{E}[\cdot]$ as it is standard in empirical process theory. Our goal is therefore to show that

$$\underbrace{(\mathbb{P}_n - \mathbb{P})(\Delta_i)}_{T_1} + \underbrace{\mathbb{P}(\Delta_i)}_{T_2} = o_{\mathbb{P}}(n^{-1/2}). \quad (22)$$

Controlling the term T_1 The first term T_1 is easy to control, as it follows directly from the following lemma.

Lemma A.1. [Kennedy et al., 2020] Let $\hat{f}(z)$ be a function estimated from a sample $Z^N = (Z_{n+1}, \dots, Z_N)$, and let \mathbb{P}_n denote the empirical measure over (Z_1, \dots, Z_n) , which is independent of Z^N . Then

$$(\mathbb{P}_n - \mathbb{P})(\hat{f} - f) = O_{\mathbb{P}}\left(\frac{\|\hat{f} - f\|}{\sqrt{n}}\right). \quad (23)$$

Since we have from assumptions that $\|\phi(\cdot; \hat{\mu}_{g(X)}, \hat{e}, g) - \phi(\cdot; \mu, e, g)\|_2^2 = o_{\mathbb{P}}(1)$, it holds that $T_1 = o_{\mathbb{P}}(n^{-1/2})$.

Controlling the term T_2 The second term requires some care. We will focus on the term involving $T_i = 1$; the case for $T_i = 0$ follows by symmetry. For $T_i = 1$, after some simple calculations, we have:

$$\begin{aligned} \Delta_i &= (\hat{\mu}_{g(X)}(W_i, 1) - \mu(W_i, 1)) + \frac{T_i}{\hat{e}(W_i)} (g(X_i) - \hat{\mu}(W_i, 1)) \\ &\quad - \frac{T_i}{e(W_i)} (g(X_i) - \mu(W_i, 1)). \end{aligned} \quad (24)$$

Note that we can drop the last term since, by assumption, g and μ are equal on average. Therefore, we can write:

$$\mathbb{E}[\Delta_i] = \mathbb{E}[\hat{\mu}_{g(X)}(W_i, 1) - \mu(W_i, 1) + \frac{1}{\hat{e}(W_i)} (g(X_i) - \hat{\mu}(W_i, 1))] \quad (25)$$

By conditional calibration, we can substitute $g(X_i)$ with $\mu(W_i, 1)$ and group:

$$\mathbb{E}[\Delta_i] = \mathbb{E}\left[(\hat{\mu}_{g(X)}(W_i, 1) - \mu(W_i, 1)) + \frac{T_i}{\hat{e}(W_i)} (\mu(W_i, 1) - \hat{\mu}_{g(X)}(W_i, 1))\right] \quad (26)$$

$$= \mathbb{E}\left[(\hat{\mu}_{g(X)}(W, 1) - \mu(W, 1)) \left(1 - \frac{T_i}{\hat{e}(W)}\right)\right] \quad (27)$$

$$= \mathbb{E}\left[(\hat{\mu}_{g(X)}(W, 1) - \mu(W, 1)) \frac{\hat{e}(W) - T_i}{\hat{e}(W)}\right]. \quad (28)$$

Conditioning on W_i we obtain:

$$\mathbb{E}[\Delta_i] = \mathbb{E}\left[\left(\frac{e(W)}{\hat{e}(W)} - 1\right) (\mu(W, 1) - \hat{\mu}_{g(X)}(W, 1))\right]. \quad (29)$$

To bound this term, we use the positivity assumption that $\hat{e}(W) \geq \epsilon > 0$ for some constant ϵ :

$$|\mathbb{E}[\Delta_i]| \leq \mathbb{E}\left[\left|\frac{e(W) - \hat{e}(W)}{\hat{e}(W)}\right| \cdot |\mu(W, 1) - \hat{\mu}_{g(X)}(W, 1)|\right] \quad (30)$$

$$\leq \frac{1}{\epsilon} \mathbb{E}[|e(W) - \hat{e}(W)| \cdot |\mu(W, 1) - \hat{\mu}_{g(X)}(W, 1)|]. \quad (31)$$

Applying Cauchy-Schwarz inequality:

$$\frac{1}{\epsilon} \mathbb{E}[|e(W) - \hat{e}(W)| \cdot |\mu(W, 1) - \hat{\mu}_{g(X)}(W, 1)|] \leq \frac{1}{\epsilon} \|e - \hat{e}\|_2 \|\mu(\cdot, 1) - \hat{\mu}_{g(X)}(\cdot, 1)\|_2. \quad (32)$$

If the estimators \hat{e} and $\hat{\mu}$ achieve suitable convergence rates such that their product of L_2 norms is $o_{\mathbb{P}}(n^{-1/2})$, then:

$$\frac{1}{\epsilon} \|e - \hat{e}\|_2 \|\mu(\cdot, 1) - \hat{\mu}_{g(X)}(\cdot, 1)\|_2 = o_{\mathbb{P}}(n^{-1/2}). \quad (33)$$

This completes the proof. \square

A.3 Proof of Theorem 3.1

Theorem (Causal Lifting transfers causal validity). *Given two similar PPCI problems \mathcal{P} and \mathcal{P}' with standard causal identification assumptions. Let $g = h \circ \phi : \mathcal{X} \rightarrow \mathcal{Y}$ be an outcome model for \mathcal{P}' with h Bayes-optimal, and assume that the representation transfers, i.e., $\mathbb{P}(\phi(X)|Y) = \mathbb{P}'(\phi(X)|Y)$. Then the Causal Lifting constraint on \mathcal{P} implies g is valid on \mathcal{P} .*

Intuition: The theorem shows that Causal Lifting, supported by other transferability assumptions, guarantees to transfer validity among PPCI problems, regardless of potential shifts in the joint distribution of (Z, Y) , e.g., different treatment effect. The core of the proof relies on establishing a hard representation transferability, i.e., $\mathbb{P}(\phi(X)|Y, Z) = \mathbb{P}'(\phi(X)|Y, Z)$, given by the assumed representation transferability (on standalone Y) and the causal lifting constraint. This is done within the expectation of the conditional calibration, which we have already shown implies validity. Note that, indeed, the (marginal) representation transferability, conditioning over Y alone, does not guarantee transferability conditioning over Z too, potentially due by systematic biases within the encoder (e.g., fully retrieving the outcome signal for a certain subgroup and partially missing it for others).

Proof. First, let us remark that if $\mathcal{P} = \mathcal{P}'$, then Bayes optimality is sufficient for validity. Therefore, we now only focus on the true generalization setting with $\mathcal{P} \neq \mathcal{P}'$. By Lemma 2.1 it is sufficient to show conditional calibration to show the outcome model causal validity. Then, by linearity of the expected value we aim to show:

$$\mathbb{E}_Y[Y | Z] \stackrel{a.s.}{=} \mathbb{E}_X[h(\phi(X)) | Z], \quad (34)$$

where $Z = [T, \tilde{W}]$, and \tilde{W} is a valid adjustment set. By the tower rule, we can expand the RHS:

$$\mathbb{E}_X[h(\phi(X)) | Z] \stackrel{a.s.}{=} \mathbb{E}_Y \left[\underbrace{\mathbb{E}_X[h(\phi(X)) | Y, Z]}_{\zeta(Y, Z)} | Z \right]. \quad (35)$$

By assumptions $\forall y \in \mathcal{Y}, z \in \mathcal{Z}$:

$$\zeta(y, z) := \mathbb{E}_X[h(\phi(X)) | Y = y, Z = z] = \quad (36)$$

$$= \mathbb{E}_X[h(\phi(X)) | Y = y] = \quad (\text{Casual Lifting constraint}) \quad (37)$$

$$= \mathbb{E}'_X[h(\phi(X)) | Y = y] = \quad (\text{representation transfers}) \quad (38)$$

$$= \mathbb{E}'_X[\mathbb{E}'_Y[Y | \phi(X)] | Y = y] = \quad (\text{Bayes-optimal predictor}) \quad (39)$$

$$= \mathbb{E}_X[\underbrace{\mathbb{E}'_Y[Y | \phi(X)]}_{\text{function of } \phi(X)} | Y = y] = \quad (\text{representation transfers}) \quad (40)$$

$$= \mathbb{E}_X[\mathbb{E}'_Y[Y | X] | Y = y] = \quad (\text{sufficiency}) \quad (41)$$

$$= \mathbb{E}_X[\mathbb{E}_Y[Y | X] | Y = y] = \quad (\text{similarity}) \quad (42)$$

$$= y \quad (\text{law of iterated expectations}) \quad (43)$$

Where with the expected value with superscript prime we refer to the expected value over the data distribution of the problem \mathcal{P}' . Substituting back $\zeta(Y, Z)$ we have the thesis. \square

B IStAnt

In this Section, we describe in detail our procedure to test zero-shot PPCI on IStAnt dataset, by designing and recording a similar experiment for finetuning.

B.1 Similar experiment and data recording (ours)

We run an experiment very much alike the IStAnt experiment with triplets of worker ants (one treated focal ant, and two nestmate ants), following the step-by-step design described their Appendix C [Cadei et al., 2024]. We recorded 5 batches of 9 simultaneously run replicates with similar background pen marking for the dish palettes positioning, producing 45 original videos, of which one had to be excluded for experimental problems, leaving 44 analyzable videos. Then, for each video, grooming events from the nestmate ants to the focal ant were annotated by a single domain expert, and we focus on the ‘or’ events, i.e., “Is one of the nestmate ants grooming the focal one?”. We used a comparable experimental setup (i.e., camera set-up, random treatment assignment, etc.) except for the following, guaranteeing invariant annotation mechanism, i.e., *similar* experiment.

- **Treatments:** Whereas IStAnt used two micro-particle applications⁵, our experimental treatments also constitute micro-particle application in two different treatments ($n = 15$ each), but also one treatment completely free of micro-particles (control, $n = 14$), all applied to the focal ant. The three treatments of the ants are visually indistinguishable, independent of micro-particle application.
- **Light conditions:** We created a lower-quality illumination of the nests by implementing a ring of light around the experiment container, resulting in more inhomogeneous lighting and a high-lux (“cold”) light effect, compared to the light diffusion by a milky plexiglass sheet proposed in the original experiment. Also, our ant nests had a higher rim from the focal plane where the ants were placed, causing some obscuring of ant observation along the walls. See a comparison of the filming set-up and an example of the resulting recording in Figure 3. We also considered a slightly lower resolution, i.e., 700x700 pixels.
- **Longer Videos:** Whereas IStAnt annotated 10 min long videos, we here annotated 30 min long videos, even if the grooming activity of the ants decreases with time after exposure to treatment. Our videos were recorded at 30fps, totaling 158 400 annotated frames in the 44 videos.
- **Other potential distribution shifts:** Other sources of variations from the original experiment are:
 - Whereas IStAnt used orange and blue color dots, we used yellow and blue.
 - Whereas in IStAnt, grooming presence or absence was annotated for each frame, we here annotated a single grooming event even if the ant stopped grooming for up to one second but then kept grooming after that, with no other behaviors being performed in between. This means that intermediate frames between grooming frames were also annotated as grooming despite the ant pausing its behavior. Such less exact grooming annotations are faster to perform for the human annotator.
 - The person performing annotation in this experiment was different from the annotators in the IStAnt dataset, leading to some possible observer effects.

Let’s observe that our work models the general pipeline in ecological experiments, where multiple experiment variants are recorded over time, e.g., upgrading the data acquisition technique, and we aim to generalize from a lower to higher quality *similar* experiment.

B.2 Zero-shot PPCI

We considered the full dataset so recorded for finetuning a pre-trained Vision Transformer, i.e., ViT-B [Dosovitskiy et al., 2020], ViT-L [Zhai et al., 2023], CLIP-ViT-B,-L [Radford et al., 2021], DINOv2 [Oquab et al., 2023], as proposed by Cadei et al. [2024] and we left IStAnt for testing causal estimation performances relying on artificial predictions. For each pre-trained encoder, we fine-tuned a multi-layer perception head (2 hidden layers with 256 nodes each and ReLU activation) on top of its *class* token via Adam optimizer ($\beta_1 = 0.9, \beta_2 = 0.9, \epsilon = 10^{-8}$) for ERM, vREx (finetuning the invariance constraint in $\{0.01, 0.1, 1, 10\}$) and DERM (ours) for 15 epochs and batch size 256. So, we fine-tuned the learning rates in $[0.0005, 0.5]$, selecting the best-performing hyper-parameters for each model-method, minimizing the Treatment Effect Bias on the

⁵By author correspondence.

training sample, while guaranteeing good predictive performances, i.e., accuracy greater than 0.8, on a small validation set (1 000 random frames). We computed the ATE at the video level (aggregating the predictions per frame) via the AIPW estimator. We used XGBoost for the model outcome and estimated the propensity score via sample mean (constant) since the treatment assignments are randomized, i.e., RCT. For the outcome model, we consider the following experiment settings for controlling: experiment day, time of the day, batch, position in the batch, and annotator. We run all the analyses using 48GB of RAM, 20 CPU cores, and a single node GPU (NVIDIA GeForce RTX2080Ti). The main bottleneck in the analysis is the feature extraction from the pre-trained Vision Transformers. We estimate 72 GPU hours to run the full analysis, despite given a candidate outcome model g already finetuned the standalone prediction-powered causal inference component, excluding feature extraction on the target experiment takes less than a GPU minute.

C CausalMNIST

To exhaustively validate our method, we replicated the comparison between DERM (our) enforcing the Causal Lifting constraint and ERM (baseline), vREx and IRM (invariant trainings) in a controlled setting, manipulating the MNIST dataset with coloring, allowing us to (i) cheaply replicate fictitious experiments several times, bootstrapping confidence intervals, and (ii) control the underlying causal effects (only empirically estimated in real-world experiments).

C.1 Data Generating Process

We considered the following training data distribution \mathbb{P}^A :

$$W = Be(0.5) \quad (44)$$

$$U = Be(0.02) \quad (45)$$

$$T = Be(0.5) \quad (46)$$

$$Y = W \cdot \text{Unif}(\{0, 1, 2, 3\}) + T \cdot \text{Unif}(\{0, 1, 2, 3\}) + U \cdot \text{Unif}(\{0, 1, 2, 3\}) \quad (47)$$

$$X := f_X(T, W, Y, U, n_X) \quad (48)$$

representing a Randomized Controlled Trial where f_X is a deterministic manipulation of a random digit image n_X from MNIST dataset enforcing the background color W (red or green) and pen color T (black or white) and padding size U (0 or 8). By exchangeability assumption:

$$\begin{aligned} \text{ATE} &= \mathbb{E}[Y|do(T=1)] - \mathbb{E}[Y|do(T=0)] = \\ &= \mathbb{E}[Y|T=1] - \mathbb{E}[Y|T=0] \\ &= 1.5 \end{aligned} \quad (49)$$

Six examples of colored handwritten digits from CausalMNIST are reported in Figure 4.



Figure 4: Random samples from a CausalMNIST sample.

Then, we considered the generic *similar* target Observational Study, with distribution:

$$W = Be(p_W) \quad (50)$$

$$U = Be(p_U) \quad (51)$$

$$T = Be(0.1) \cdot (1 - W) + Be(0.9) \cdot W \quad (52)$$

$$X := f_X(T, W, Y, U, n_X) \quad (53)$$

with *linear* outcome/effect (null):

$$Y = W \cdot \text{Unif}(\{0, 1, 2, 3\}) + \text{Unif}(\{0, 1, 2, 3\}) + U \cdot \text{Unif}(\{0, 1, 2, 3\}) \quad (54)$$

where simply:

$$\text{ATE} = \mathbb{E}[Y|do(T=1)] - \mathbb{E}[Y|do(T=0)] = 0 \quad (55)$$

and *non-linear* outcome/effect:

$$Y = (T \vee U) \cdot \text{Unif}(\{0, 1, 2, 3\}) + \text{Unif}(\{0, 1, 2, 3, 4, 5, 6\}) \quad (56)$$

with respect to the experimental settings, where, by adjustment formula:

$$\begin{aligned} \text{ATE} &= \mathbb{E}[Y|do(T=1)] - \mathbb{E}[Y|do(T=0)] = \\ &= P(U=0) \cdot (\mathbb{E}[Y|T=1, U=0] - \mathbb{E}[Y|T=0, U=0]) = \\ &= (1 - p_U) \cdot 1.5 \end{aligned} \quad (57)$$

and we considered 4 different instances \mathbb{P}^B , \mathbb{P}^C , \mathbb{P}^D and \mathbb{P}^E varying the outcome model and experimental settings parameters. \mathbb{P}^B and \mathbb{P}^C have null effect, while \mathbb{P}^D and \mathbb{P}^E have heterogeneous effect. \mathbb{P}^B and \mathbb{P}^D are closer in distribution to the training since $p_U \ll 1$, while \mathbb{P}^C and \mathbb{P}^E are more out-of distribution since the padding variable U is balanced, i.e., $p_U = 0.5$, but during training it is rarely observed activated. For simplicity we refer to \mathbb{P}^B as the distribution of the the target experiment population with linear effect and “soft” (experimental settings) shift, \mathbb{P}^C with linear effect and “hard” shift, \mathbb{P}^D with non-linear effect and “soft” shift, \mathbb{P}^E with non-linear effect and “hard” shift. In Table 2 we summarize the different distribution parameters, also reporting the corresponding (exact) ATE value.

Table 2: Summary of the training and target experiment distributions.

In-Distribution		OoD (<i>linear effect</i>)		OoD (<i>non-linear effect</i>)	
		Soft shift	Hard shift	Soft shift	Hard shift
Distribution	\mathbb{P}^A	\mathbb{P}^B	\mathbb{P}^C	\mathbb{P}^D	\mathbb{P}^E
p_W	0.5	0.05	0.5	0.2	0.5
p_U	0.02	0.05	0.5	0.2	0.5
Randomized	True	False	False	False	False
Effect	Linear	Null	Null	Non Linear	Non Linear
ATE	1.5	0	0	1.2	0.75

These data generating processes represent fictitious experiments where we aim to quantify the effect of the pen color on the number to draw (if asked to pick one), relying on a machine learning model for handwritten-digits classification. Particularly, the shift in the treatment effect between training (ATE= 1.5) and target population (ATE $\in \{0, 0.75, 1.2\}$), may be interpreted as (i) testing a different, still homogeneous group of individuals, or (ii) varying the effect by changing the brand of the pens, unobserved variable (perfectly retrievable by the pen color on the training distribution), while keeping the same colors, reflecting the crucial challenges described in Section 2.1.

C.2 Analysis

We sampled 10 000 observations from \mathbb{P}^A to train a digits classifier (a Convolutional Neural Network) and tested it in PPCI in-distribution (10 000 more sample from \mathbb{P}^A) and out-of-distribution (zero-shot) on 10 000 observations for each \mathbb{P}^B , \mathbb{P}^C , \mathbb{P}^D , \mathbb{P}^E . We replicated the modeling choices for CausalMNIST proposed in Cadei et al. [2024] and described in their Appendix E.2 (without relying on pre-trained models). Particularly, the proposed network consists of two convolutional layers followed by two fully connected layers. The first convolutional layer applies 20 filters of size 5x5 with ReLU activation, followed by a 2x2 max-pooling layer. The second convolutional layer applies 50 filters of size 5x5 with ReLU activation, followed by another 2x2 max-pooling layer. The output feature maps are flattened and passed to a fully connected layer with 500 neurons and ReLU activation. The final fully connected layer reduces the output to ten logits (one per digit) on which we apply a softmax activation to model the probabilities directly. Table 3 reports a full description of the training details for such network. Particularly we tuned the number of epochs in $\{10, 11, \dots, 50\}$ and learning rate in $\{0.01, 0.001, 0.0001, 0.00001\}$ by minimizing the Mean Squared Error on a small validation set (1 000 images) and finally retraining the model on the full training sample with the optimal parameters.

Table 3: Training details for the Convolutaional Neural Network training on CausalMNIST.

Hyper-parameters		Value
Loss	Cross Entropy	
Learning Rate	0.0001	
Optimizer	Adam ($\beta_1 = 0.9, \beta_2 = 0.9, \epsilon = 10^{-8}$)	
Batch Size	32	
Epochs	40	

For each learning objective, i.e., DERM (ours), ERM, vREx and IRM, we trained a model on the training sample, imputed the outcome in each target sample and estimated the ATE via AIPW. Within the AIPW estimator we used the XGBoost regressor for the outcome regression and the XGBoost classifier to estimate the propensity score on observational studies (or vanilla sample mean on randomized controlled trials since constant). For both IRM and vREx we replicated the same hyper-parameter tuning of the invariant coefficient from our experiments on ISTAnt generalization, selecting in both case the invariant coefficient $\lambda = 0.1$. We repeated each experiment 50 times, including resampling the data, and bootstrapped the confidence interval of the ATE estimates. We run all the analysis using 10GB of RAM, 8 CPU cores, and a single node GPU (NVIDIA GeForce RTX2080Ti). The main bottleneck of each experiment is re-generating a new version of CausalMNIST from MNIST dataset, and then training the model. The Prediction-Powered ATE estimation is significantly faster. We estimate a total of 12 GPU hours to reproduce all the experiments described in this section.